

1  
2 **Early stages of decomposition within the  $\gamma'$  phase of a Ni-Al-Ti model alloy**  
3  
4

5 **F. Vogel<sup>a,\*</sup>, N. Wanderka<sup>a</sup>, S. Matsamura<sup>b</sup> and J. Banhart<sup>a</sup>**  
6

7  
8 *<sup>a</sup> Helmholtz Zentrum Berlin GmbH, Hahn-Meitner Platz 1, 14109 Berlin, Germany*  
9

10 *<sup>b</sup> Department of Applied Quantum Physics and Nuclear Engineering, Kyushu University,*  
11  
12 *Fukuoka 819-0395, Japan*  
13  
14

15  
16 **Abstract**  
17

18  
19  
20 A Ni-8.5Al-5.4Ti (at.%) model alloy was subjected to a two-step heat treatment resulting in  
21  
22 the formation of  $\gamma'$  precipitates in a  $\gamma$  matrix. The microstructural evolution was followed by  
23  
24 transmission electron microscopy. Atom probe analyses at the nanometre scale showed the  
25  
26 inhomogeneous distribution of Ni, Al and Ti in the  $\gamma'$  precipitates. Ni-rich and Ni-depleted  
27  
28 clusters were observed. The results are discussed with respect to the excess of Ni within the  $\gamma'$   
29  
30 phase based on the conditions of heat treatment.  
31  
32  
33  
34  
35  
36  
37  
38  
39

40 **Keywords** A. nickel aluminides, based on Ni<sub>3</sub>Al ; A. ternary alloy systems ; B. precipitates ;  
41  
42 F. atom probe ; F. electron microscopy, transmission ; G. aero-engine components;  
43  
44  
45

46 \* Corresponding author: F. Vogel, email: [florian.vogel@helmholtz-berlin.de](mailto:florian.vogel@helmholtz-berlin.de), Tel: +49 30 8062 43217, FAX: +49  
47  
48 30 8062 3059  
49  
50  
51  
52  
53  
54  
55  
56  
57  
58  
59  
60  
61  
62  
63  
64  
65

## 1. Introduction

Ni-based superalloys are highly heat-resistant materials used for disks and blades in turbine engines. Appropriate heat treatment of such alloys leads to the formation of a two-phase microstructure which consists of coherent  $\gamma'$  precipitates ( $L1_2$ -ordered) embedded in a  $\gamma$  solid solution matrix (A1-disordered). This two-phase microstructure is crucial for creep and fatigue resistance at high temperatures. The strength of Ni-based superalloys is mainly determined by the  $\gamma'$  precipitates. However, under service conditions at elevated temperature, the cuboidal  $\gamma'$  precipitates coarsen directionally and form rafts [1]. Although it has been controversially discussed in the past [2-4], it is generally well accepted that this morphological change of  $\gamma'$  precipitates deteriorates creep resistance and thus reduces the lifetime of these materials [4-10].

Since the introduction of Ni-based superalloys in the 1940s there has been a remarkable development of this class of alloys, leading from polycrystalline to single crystal materials and shifting the maximum operating service temperature from 1173 K for first generation materials to about 1373 K for modern alloys [11]. However, the search for even further improved Ni-based alloys still continues due to their multiple advantages, e.g. creep rupture strength, despite advances in other materials, e.g.  $\gamma$  TiAl alloys [12].

Recently, a novel separation phenomenon in the  $\gamma'$  phase has been reported, namely precipitation of  $\gamma$  particles within the  $\gamma'$  precipitates during ageing after the homogenization heat treatment [13-15]. Such phase separation was not only observed in the ternary system Ni-Al-Ti [14, 15] which still remains one of the most important systems in superalloy metallurgy [16], but also in the ternary alloys Ni-Al-Fe [17], Ni-Si-Fe [17] and Ni-Al-Si [18].

Precipitation of  $\gamma$  within the  $\gamma'$  phase and the successive division of cuboidal  $\gamma'$  precipitates into smaller units result in a significant retardation of microstructure coarsening [15]. The evolution of the morphology of those  $\gamma$  precipitates within the  $\gamma'$  phase of ternary Ni-8.5Al-

1 5.4Ti (at.%) alloy has been elaborated by transmission electron microscopy (TEM) [14] and  
2  
3 transmission electron tomography imaging [15]. However, neither the mechanism of  $\gamma$   
4  
5 precipitation within  $\gamma'$  precipitates is fully understood nor has the chemical composition of the  
6  
7 newly formed  $\gamma$  particles been reported.  
8  
9

10 In the present study, the early stages of decomposition of  $\gamma'$  precipitates in a Ni-8.5Al-  
11  
12 5.4Ti (at.%) model alloy were investigated by three-dimensional atom probe (3D-AP). In  
13  
14 addition, information on the evolution of the two-phase microstructure was obtained by  
15  
16 transmission electron microscopy.  
17  
18  
19  
20  
21  
22  
23

## 24 **2. Experimental**

25  
26  
27 A model alloy with a nominal composition of Ni-8.5Al-5.4Ti (at.%) with a purity of  
28  
29 alloying elements of 4N, 5N and 4N, respectively, was produced in an argon atmosphere  
30  
31 ( $2 \times 10^{-3}$  Pa) using an induction furnace. After casting, the ingots were cut into plates (about.  
32  
33 10 x 20 x 1 mm) and the samples were heat treated at 1213 K for 45 minutes and subsequently  
34  
35 aged at 1023 K for 6, 12 and 48 h in a quenching furnace under flowing argon. All heat  
36  
37 treatments were followed by rapid removal from furnace and quenching in ice water. In order  
38  
39 to observe the early stages of decomposition the pre-aging at temperatures above 1213 K was  
40  
41 avoided in the present study which is different to the heat treatment used in Ref.'s [14, 15].  
42  
43  
44  
45  
46

47 For transmission electron microscopy, discs of 3 mm diameter were punched out of the  
48  
49 aged samples. Thin foils suitable for TEM were prepared by electrolytic jet polishing in a  
50  
51 solution of 10% perchloric acid in 90% ethanol with 7 g thiourea at 253 K [19]. TEM  
52  
53 measurements were carried out using a Philips CM30 microscope operating at 300 kV.  
54  
55  
56

57 Square rods of  $0.2 \times 0.2 \times 10 \text{ mm}^3$  volume were cut out of the aged samples. Needle-  
58  
59 shaped tips with a radius  $< 50 \text{ nm}$  for 3D-AP analysis were prepared by electropolishing at  
60  
61  
62  
63  
64  
65

1 room temperature at a DC-voltage of about 15 V in two steps: 1) electropolishing in a solution  
2 of 15% perchloric acid in acetic acid; 2) micro-electropolishing using an electrolyte of 2%  
3 perchloric acid in butoxyethanol [19]. 3D-AP analyses were performed using a TAP,  
4 CAMECA [20], with instrument parameters of ultra-high vacuum  $p < 10^{-6}$  Pa, a pulse-to-DC-  
5 voltage ratio of 0.2, a pulse repetition frequency of 1 kHz and a tip temperature of about 70 K.  
6  
7  
8  
9  
10  
11  
12  
13  
14  
15

### 16 3. Results and Discussion

17  
18 The bright-field (BF) TEM micrograph of the Ni-Al-Ti alloy after heat treatment at  
19 1213 K for 45 min shown in Fig. 1a exhibits a microstructure without visible  $\gamma'$  precipitates.  
20  
21 The corresponding selected area diffraction (SAED) pattern shows  $L1_2$  superlattice reflections  
22 indicating long range order (LRO). The small dark regions indicated by arrows represent  
23 ordered areas. Typical microstructures of the alloy after the two-step heat treatments applied  
24 are shown in the BF-TEM micrographs displayed in Fig. 1b-c. A two-phase microstructure  
25 comprising a  $\gamma$  matrix and  $\gamma'$  precipitates is formed. The edges of the cuboidal  $\gamma'$  precipitates  
26 are aligned along various  $\langle 001 \rangle$  directions. The corresponding SAED patterns are shown in  
27 the insets of Fig. 1b-d. The electron diffraction pattern of the  $[001]$  zone axis exhibits  
28 superlattice reflections from  $\gamma'$  precipitates. The  $\gamma'$  phase is coherent with the fcc  $\gamma$  matrix.  
29 The strain contrast surrounding the  $\gamma'$  particles is due to a lattice mismatch between  $\gamma$  matrix  
30 and  $\gamma'$  phase. This behaviour is visible in BF-TEM images, whereas Dark Field (DF) imaging  
31 is not sensitive to strain contrast [21].  
32  
33  
34  
35  
36  
37  
38  
39  
40  
41  
42  
43  
44  
45  
46  
47  
48  
49  
50

51 Fig. 2a exhibits a three-dimensional reconstruction of Ti atom positions in an analyzed  
52 volume of  $8.7 \times 8.7 \times 105.0$  nm<sup>3</sup> of the specimen aged at 1023 K for 48 h. Two regions are  
53 visible, a Ti-depleted and a Ti-enriched area, corresponding to the  $\gamma$  and  $\gamma'$  phase,  
54 respectively. Ni and Al atoms have been omitted in this figure for reasons of clarity. The  
55  
56  
57  
58  
59  
60  
61  
62  
63  
64  
65

1 average chemical compositions of  $\gamma$  and  $\gamma'$  phases for each ageing state are given in Table 1.

2  
3 The calculated volume fraction of the  $\gamma'$  phase from 3D-AP data,  $V_{\gamma'}$ , is also listed.

4  
5 Compositions and the volume fraction were found to have reached a constant state after 6 h of  
6  
7 ageing.  
8  
9

10 Fig. 2b illustrates concentration depth profiles of all alloying elements evaluated along a  
11 cylinder of 3 nm diameter aligned along the centre of the reconstructed volume shown in Fig.  
12 2a. The concentration values were calculated for cylinder slices of 0.5 nm thickness (i.e. a  
13 volume of  $\sim 3.5 \text{ nm}^3$ ) and each data point represents about 100 atoms. The concentration  
14  
15 depth profiles of all elements in the  $\gamma'$  phase indicate real fluctuations in concentration since  
16  
17 they exceed the statistical error  $2\sigma$ .  
18  
19  
20  
21  
22  
23  
24  
25

26 In order to quantify the inhomogeneous distribution of alloying elements within the  $\gamma'$   
27 phase, a statistical analysis, namely the cluster search module [22], was applied. The results of  
28  
29 the analysis of clusters, composed of Ni, Al and Ti atoms, are shown in Fig. 3. Clusters  
30  
31 containing more than 82 at.% Ni are shown within the  $\gamma'$  phase in specimens aged for a) 6 h,  
32  
33 b) 12 h and c) 48 h. In later stages, the ensemble of clusters appears to be interconnected,  
34  
35  
36 indicating the early stages of decomposition towards  $\gamma$  precipitation. The chemical  
37  
38 compositions of Ni-enriched and Ni-depleted regions are listed in Table 2.  
39  
40  
41  
42  
43

44 The nominal composition of the investigated alloy ( $C_{nom}$ ), as well as the chemical  
45  
46 compositions of  $\gamma$  and  $\gamma'$  phases after heat treatment as measured by 3D-AP are plotted in a  
47  
48 calculated ternary phase diagram, shown in Fig. 4a as an isothermal section at 1023 K [23].  
49  
50 The chemical compositions of  $\gamma'$  phases after all ageing times investigated are all located well  
51  
52 within the calculated  $\gamma'$  phase existence area. The chemical compositions of Ni-enriched and  
53  
54 Ni-depleted clusters within the  $\gamma'$  phase are also shown. Obviously, the chemical  
55  
56  
57  
58  
59  
60  
61  
62  
63  
64  
65

1 compositions of these Ni-rich and Ni-depleted clusters are located outside the  $\gamma'$  phase  
2  
3 existence area.  
4

5  
6 Recently published studies of the same alloy demonstrated the formation of  $\gamma$  precipitates  
7  
8 within the  $\gamma'$  phase [14, 15], whereas, in the present study, only clusters rich or depleted in Ni  
9  
10 were found. This discrepancy can be explained by the different heat treatments of the alloys  
11  
12 investigated. A two-step heat treatment with preceding homogenization was applied in Ref.'s  
13  
14 14 and 15, whereas in the present work, the two-step heat treatment alone was performed,  
15  
16 without preceding homogenization. Initial homogenization of the Ni-Al-Ti alloy in Ref.'s 14  
17  
18 and 15 was performed at a temperature not explicitly specified but believed to be higher than  
19  
20 1213 K (in the  $\gamma$  single phase region) aiming at obtaining an Al (fcc) solid solution. An  
21  
22 already established  $\gamma/\gamma'$  microstructure after homogenization at 1473 K for 1h was observed in  
23  
24 the present study (not shown here). In contrast, the heat treatment at 1213 K for 45 min  
25  
26 without preceding homogenization leads to the formation of a microstructure shown in Fig.  
27  
28 1a. In order to slow down the  $\gamma'$  precipitation, the homogenization was omitted in this work.  
29  
30 Therefore, the microstructure after ageing at 1213 K for 45 min was also different when  
31  
32 compared with that in Ref.'s 14 and 15. Whereas in the present study only the very early  
33  
34 stages of  $\gamma/\gamma'$  separation are shown (Fig. 1a), the alloy in Ref.'s 14 and 15 contained cuboidal  
35  
36  $\gamma'$  precipitates, representing more advanced stages of ageing. Furthermore, this difference in  
37  
38 heat treatment is the reason why in the present study only clusters were found within the  $\gamma'$   
39  
40 phase and not  $\gamma$  precipitates as obtained in Ref.'s 14 and 15 after ageing at 1023 K.  
41  
42  
43  
44  
45  
46  
47  
48  
49  
50

51  
52 A qualitative comparison with results of Tian et al. [24], shows that solubility of Ni in the  
53  
54  $\gamma'$  phase could be responsible for phase separation. They reported the temperature dependence  
55  
56 of the boundary between  $\gamma'$  single-phase region and ( $\gamma+\gamma'$ ) two-phase region of a Ni-Al-Ti  
57  
58 alloy system as a function of (Al+Ti) and Ni content (see Fig. 4b). The Ti/Al ratio of their  
59  
60  
61  
62  
63  
64  
65

1 alloy is 0.77 in contrast to 0.64 for the alloy of the present work. For example, the boundary  
2 shifts from about 78.8 at.% of Ni at 1213 K to 77.5 at.% at 1023 K. Thus, the solubility limit  
3 of Ni within the  $\gamma'$  phase decreases as the temperature decreases. In Ref.'s 14 and 15 a higher  
4 amount of Ni is expected in the  $\gamma'$  phase as a result of the homogenization treatment applied at  
5 a temperature above 1213 K. In those experiments, the first and second steps of aging were  
6 performed at 1213 K and 1023 K, respectively. Hence, at temperatures below 1213 K, the  
7 excess of Ni within the  $\gamma'$  phase will be reduced [24] in order to reach a local equilibrium state  
8 between  $\gamma$  and ( $\gamma+\gamma'$ ) regions. This explanation also accounts for the decomposition of the  $\gamma'$   
9 phase towards Ni-enriched and Ni-depleted regions observed in the present study. The excess  
10 of Ni in the  $\gamma'$  phase was lower compared to that in Ref.'s 14 and 15 due to absence of the  
11 homogenization treatment (which would inherently lead to the precipitate formation of  $\gamma'$   
12 particles). Instead of  $\gamma$  particles within the  $\gamma'$  phase, in this study, Ni-rich and Ni-depleted  
13 clusters were observed and their formation can be interpreted as the early stages of  
14  $\gamma$  precipitation within the  $\gamma'$  phase.  
15  
16  
17  
18  
19  
20  
21  
22  
23  
24  
25  
26  
27  
28  
29  
30  
31  
32  
33  
34  
35  
36  
37  
38

#### 39 **4. Conclusion**

40  
41  
42 The combination of TEM and 3D-AP allows to follow the evolution of the two-phase  
43 microstructure ( $\gamma'$  precipitates and the  $\gamma$  matrix) after heat treatment at 1213 K for 45 min,  
44 quenching and subsequent ageing at 1023 K for 6 h, 12 h and 48 h.  
45  
46  
47  
48  
49

50 Qualitative TEM analysis revealed  $L1_2$  superlattice reflections for every state of  
51 ageing and showed formation of  $\gamma'$  precipitates in the period from 6 h to 48 h of ageing.  
52  
53

54 Although  $\gamma$  particles within the  $\gamma'$  precipitates could not be observed, atom probe analyses on  
55 the nanometre scale showed that the distribution of Ni, Al and Ti in the  $\gamma'$  precipitates is not  
56 homogeneous. A statistical analysis of 3D-AP data of the  $\gamma'$  phases showed the existence of  
57  
58  
59  
60  
61

1 Ni-rich and Ni-depleted regions. Decomposition within the  $\gamma'$  phase was explained by the  
2  
3 temperature-dependent solubility of Ni. Its amount in the  $\gamma'$  phase reduces with decreasing  
4  
5 temperature due to a local equilibrium state between  $\gamma$  and ( $\gamma+\gamma'$ ) regions. The decomposition  
6  
7 of the  $\gamma'$  phase towards Ni-rich and Ni-depleted clusters can be seen as early stages of  $\gamma$   
8  
9 precipitation in the  $\gamma'$  phase.  
10  
11  
12  
13  
14  
15  
16  
17  
18  
19  
20  
21  
22  
23  
24  
25  
26  
27  
28  
29  
30  
31  
32  
33  
34  
35  
36  
37  
38  
39  
40  
41  
42  
43  
44  
45  
46  
47  
48  
49  
50  
51  
52  
53  
54  
55  
56  
57  
58  
59  
60  
61  
62  
63  
64  
65



## Figure captions

**Figure 1.** Bright-field TEM images of Ni-8.5Al-5.4Ti (at.%) alloy after a) heat treatment at 1213 K for 45 min, quenching and b-d) also subsequent ageing at 1023 K for b) 6 h, c) 12 h and d) 48 h. No cuboidal precipitates in a) but superlattice reflections indicate  $L1_2$  structure. Precipitates with cuboidal morphology b-d) correspond to the ordered  $\gamma'$  phase ( $L1_2$  structure). The corresponding electron diffraction patterns of the [001] zone axis are shown in the inset.

**Figure 2.** a) Three-dimensional reconstruction of a region ( $8.7 \times 8.7 \times 105 \text{ nm}^3$ ) of Ni-8.5Al-5.4Ti (at.%) alloy aged at 1023 K for 48 h containing a  $\gamma/\gamma'$  interface. For the sake of clarity only the Ti atom positions are shown. b) Concentration depth profiles of the elements Ni, Al and Ti taken along a cylinder (not shown here) of 4 nm diameter oriented parallel to the long axis of the box shown in a) and approximately perpendicular to the  $\gamma/\gamma'$  interface. The concentration values were determined in steps of 0.5 nm. The dashed line indicates the  $\gamma/\gamma'$  interface.

**Figure 3.** Three-dimensional reconstruction of Ni-rich clusters (defined as  $> 82 \text{ at.}\% \text{ Ni}$ ) within  $\gamma'$  precipitates of Ni-8.5Al-5.4Ti (at.%) alloy after heat treatment at 1213 K for 45 min, quenching and subsequent ageing at 1023 K for a) 6 h, b) 12 h and c) 48 h as evaluated using the cluster search module [22]. The inhomogeneous distribution of alloying elements within the  $\gamma'$  phase is revealed. The length of the analyzed volumes is 25 nm, the edges are a)  $7.8 \times 7.8 \text{ nm}^2$ , b)  $8.6 \times 8.6 \text{ nm}^2$  and c)  $12 \times 12 \text{ nm}^2$ . The corresponding TEM images are also shown.

1 **Figure 4.** a) Ni-Al-Ti ternary phase diagram at 1023 K after Raghavan [23]. The nominal  
2 composition  $C_{\text{nom}}$  (X, green) of the alloy investigated and the composition of  $\gamma$  and  $\gamma'$  phase  
3 after heat treatment at 1213 K for 45 min, quenching and subsequent ageing at 1023 K for 6 h  
4 (circles), 12 h (triangles) and 48 h (squares) of the present work are added. Ni-rich (blue  
5 symbols) and Ni-depleted (magenta symbols) decomposed regions in the  $\gamma'$  phases are also  
6 given. b) Quasi-binary section of a Ni-(Al+Ti) phase diagram with  $X_{\text{Ti}}/X_{\text{Al}} = 0.77$  after Tian  
7 et al. [24]. The boundary between  $\gamma'$  single-phase and  $(\gamma+\gamma')$  two-phase region of a Ni-Al-Ti  
8 alloy shows temperature dependent solubility of Ni in  $\gamma'$  phase.  
9  
10  
11  
12  
13  
14  
15  
16  
17  
18  
19  
20  
21  
22

### 23 **Table captions**

24  
25  
26  
27  
28 **Table 1.** Compositions of  $\gamma$  and  $\gamma'$  phases and the volume fraction  $V_{\gamma'}$  of the  $\gamma'$  phase in alloy  
29 Ni-8.5Al-5.4Ti (at.%) after heat treatment at 1213 K for 45 min, quenching and subsequent  
30 ageing at 1023 K. The error given is standard deviation  $2\sigma$ .  
31  
32  
33  
34  
35  
36  
37

38 **Table 2.** Compositions of Ni-rich and Ni-depleted regions within the  $\gamma'$  phase after heat  
39 treatment at 1213 K for 45 min, quenching and subsequent ageing at 1023 K. Standard  
40 deviations  $2\sigma$  are given.  
41  
42  
43  
44  
45  
46  
47  
48  
49  
50  
51  
52  
53  
54  
55  
56  
57  
58  
59  
60  
61  
62  
63  
64  
65

## References

- [1] S. Draper, D. Hull, R. Dreshfield, *Metall. Trans.* **20A**, (1989), 683-687.
- [2] J. Hammer, H. Mughrabi, *Proc. 1st Eur. Conf. On Advanced Materials and Processes*, EUROMAT'89, (Eds: D. Driver, H. Mughrabi), Informationsgesellschaft-Verlag, Oberursel, Germany, (1989), 445.
- [3] H. Mughrabi, W. Schneider, V. Sass, C. Lang, *Proc. 10th Int. Conf. Strength of Metals and Alloys*, ICSMA 10, (Eds: H. Oikawa, K. Maruyama, S. Takeuchi, M. Yamaguchi), Jpn. Inst. Metals, Sendai, Japan.
- [4] F.R.N. Nabarro, *Metall. Trans.* **27A**, (1996), 513-530.
- [5] W. Schneider, J. Hammer, H. Mughrabi in: *Superalloys 1992*, (Eds: S.D. Antolovich, R.W. Stusrud, R.A. MacKay, D.L. Anton, T. Khan, R.D. Kissinger, D.L. Klarstrom), TMS, Warrendale, PA, (1992), 589-598.
- [6] H. Mughrabi in: *The Johannes Weertman Symposium*, (Eds: R.J. Arsenault, D. Cole, T. Fross, G. Kostorz, P.K. Liaw, S. Parameswaran, H. Sizek), TMS, Anaheim, CA, (1996), 267-278.
- [7] D. Mukherji, H. Gabrisch, W. Chen, H.J. Fecht, R.P. Wahi, *Acta Mater.* **45/8**, (1997), 3143.
- [8] M. Kamaraj, *Sadhana* **28**, (2003), 115-128.
- [9] A. Epeshin, T. Link, M. Nazmy, M. Staubli, H. Klingelhöffer, G. Nolze in: *Superalloys 2008*, (Eds: R.C. Reed, K.A. Green, P. Caron, T.P. Gabb, M.G. Fahrman, E.S. Huron, S.A. Woodard), TMS, Warrendale, PA, (2008), 725-731.
- [10] T. Tinga, W.A.M. Brekelmans, M.G.D. Geers, *Comp. Mater. Sci.* **47/2**, (2009), 471-481.
- [11] H. Mughrabi, M. Ott, U. Tetzlaff, *Mater. Sci. Eng. A* **236**, (1997), 434-437.
- [12] J.C. Chesnutt in: *Superalloys 1992*, (Eds: S.D. Antolovich, R.W. Stusrud, R.A. MacKay, D.L. Anton, T. Khan, R.D. Kissinger, D.L. Klarstrom), TMS, Warrendale, PA, (1992), 381-389.
- [13] J.M. Oblak, J.E. Doherty, A.F. Giamei, B.H. Kear, *Metall. Trans.* **5**, (1973), 1252-1255.
- [14] M. Doi, D. Miki, T. Moritani, T. Kozakai, in: *Superalloys 2004*, (Eds: K.A. Green, T.M. Pollock, H. Harada, T.E. Howson, R.C. Reed, J.J. Schirra, S. Walston), TMS, Warrendale, PA, (2004), 109-114.
- [15] S. Hata, K. Kimura, H. Gao, S. Matsumura, M. Doi, T. Moritani, J.S. Banard, J.R. Tong, J.H. Sharp, P.A. Midgley, *Adv. Mater.* **20**, (2008), 1905-1909.
- [16] M.S.A. Karunaratne, P. Carter, R.C. Reed, *Acta Mater.* **49**, (2001), 861-875.
- [17] M. Senga, H. Kumagai, T. Moritani, M. Doi, *Adv. Mater. Res.* **26-28**, (2007), 1311-1314.
- [18] T. Moritani, M. Ota, T. Kozakai, M. Doi, *Mater. Sci. Forum* **561-565**, (2007), 2361-2364.
- [19] Y. Zhang, N. Wanderka, G. Schumacher, R. Schneider, W. Neumann, *Acta Mater.* **48** (2000), 2787-2793.
- [20] D. Blavette, B. Deconihout, A. Bostel, J.M. Sarrau, M. Bouet, A. Menand, *Rev. Sci. Instrum.* **64/10**, (1993), 2911-2919.
- [21] A.J. Ardell, *Metall. Trans.* **1**, (1970), 525-534.
- [22] X. Sauvage, G. Dacosta, R.Z. Valiev in: *3rd Int. Symp. On Ultrafine Grained Materials*, TMS 2004 Annual Meeting, (Eds: Y.T. Zhu, T.G. Langdon, R.Z. Valiev, S.L. Semiatin, D.H. Shin, T.C. Lowe), Charlotte, NC, (2004), 31.
- [23] V. Raghavan, *J. Phase Equilib.* **26/3**, (2005), 268.
- [24] W.H. Tian, T. Sano, M. Nemoto, *J. Jpn. Inst. Metals*, **53** (1989), 1013.

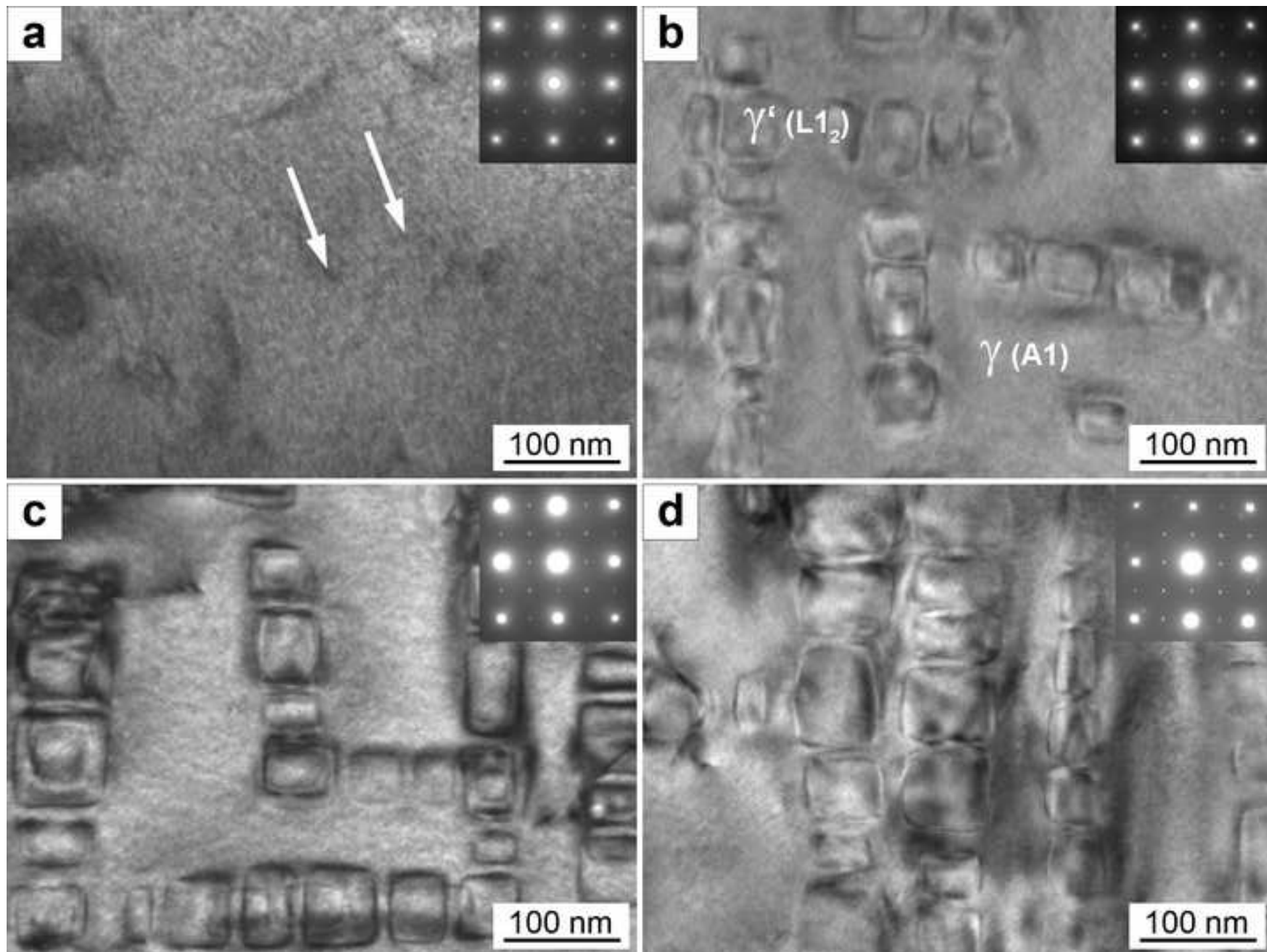
**Table 1**

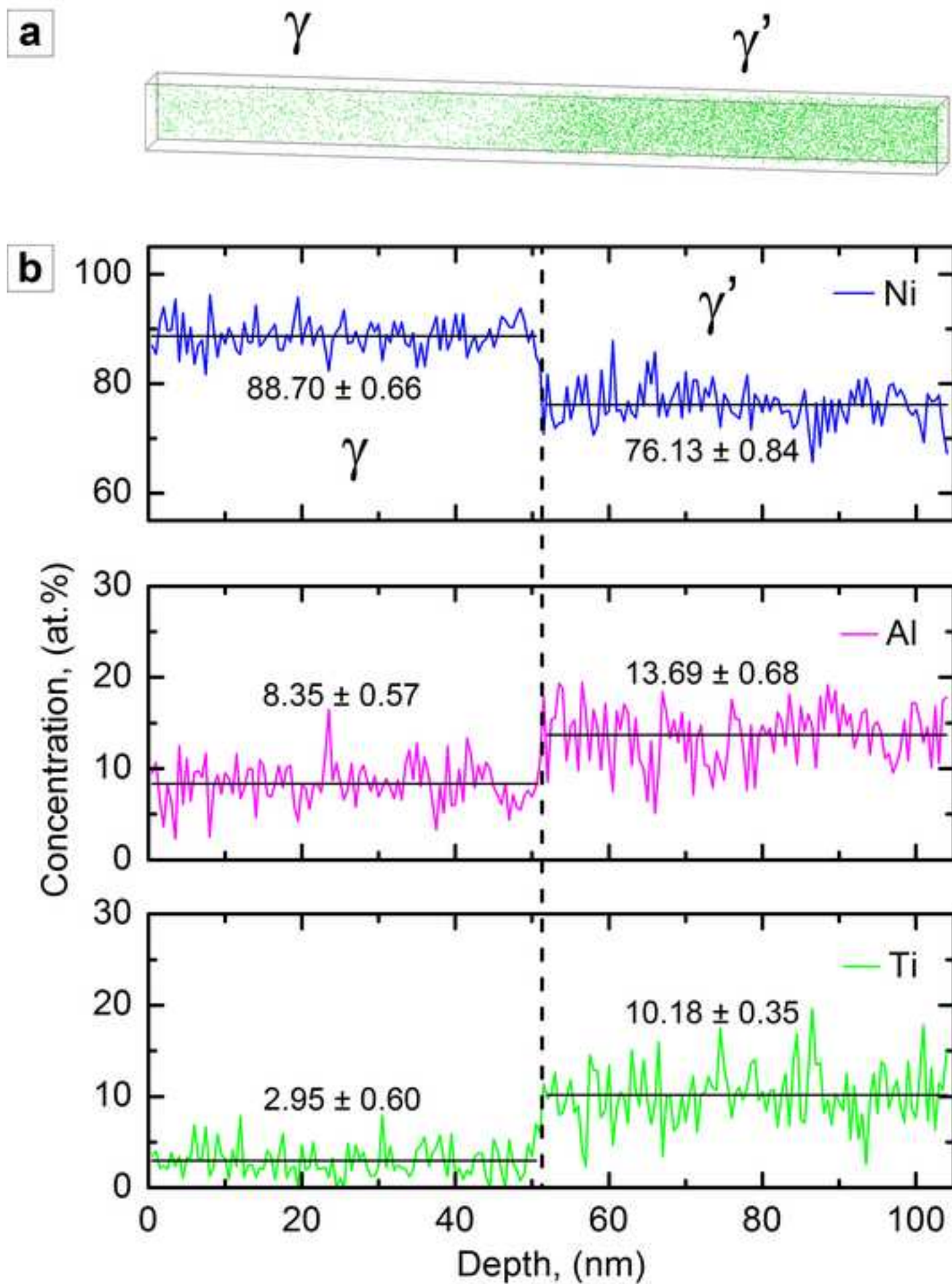
HT	$\gamma$			$\gamma'$			$V_{\gamma'}$
	Ni	Al	Ti	Ni	Al	Ti	
6 h	$90.47 \pm 0.07$	$6.59 \pm 0.06$	$2.95 \pm 0.04$	$76.94 \pm 0.43$	$13.36 \pm 0.34$	$9.71 \pm 0.30$	$32,28 \pm 0,62$
12 h	$90.61 \pm 0.49$	$6.27 \pm 0.42$	$2.67 \pm 0.27$	$74.77 \pm 0.39$	$13.56 \pm 0.31$	$11.67 \pm 0.29$	$28,50 \pm 0,33$
48 h	$90.57 \pm 0.16$	$6.95 \pm 0.14$	$2.47 \pm 0.08$	$75.41 \pm 0.10$	$14.16 \pm 0.08$	$10.44 \pm 0.07$	$29,50 \pm 1,17$

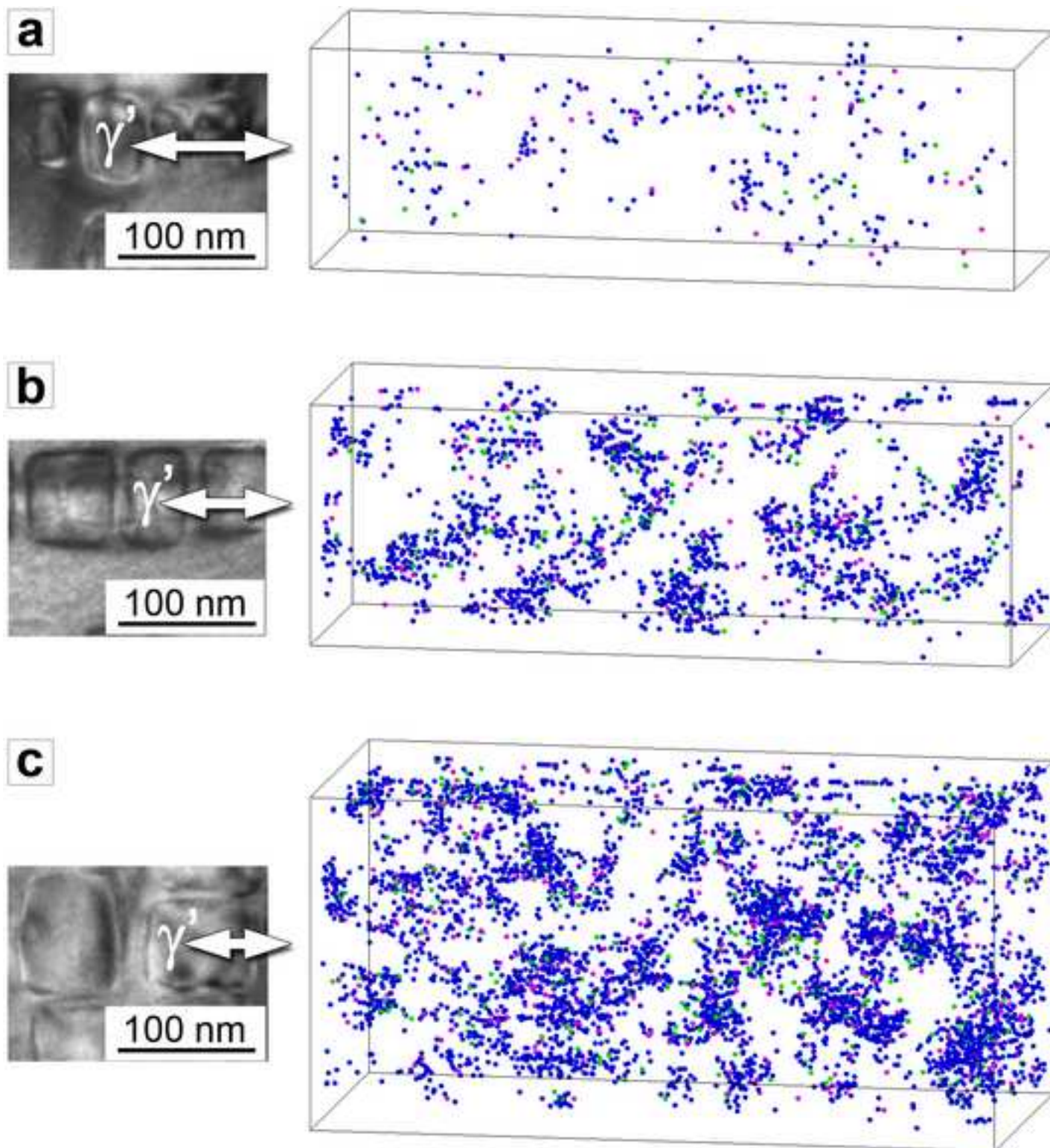
**Table 2**

ST + HT	Ni > 82 at. %			Al > 18 at. %		
	Ni	Al	Ti	Ni	Al	Ti
6 h	84.86 ± 1.14	9.18 ± 0.92	5.95 ± 0.75	71.68 ± 1.69	20.11 ± 1.07	8.21 ± 0.73
12 h	85.56 ± 1.84	7.02 ± 1.34	7.43 ± 1.38	69.39 ± 1.28	19.75 ± 1.10	10.85 ± 0.86
48 h	83.63 ± 1.16	9.12 ± 0.90	7.24 ± 0.81	68.32 ± 1.67	21.34 ± 1.47	10.33 ± 1.09

Figure(s)  
[Click here to download high resolution image](#)

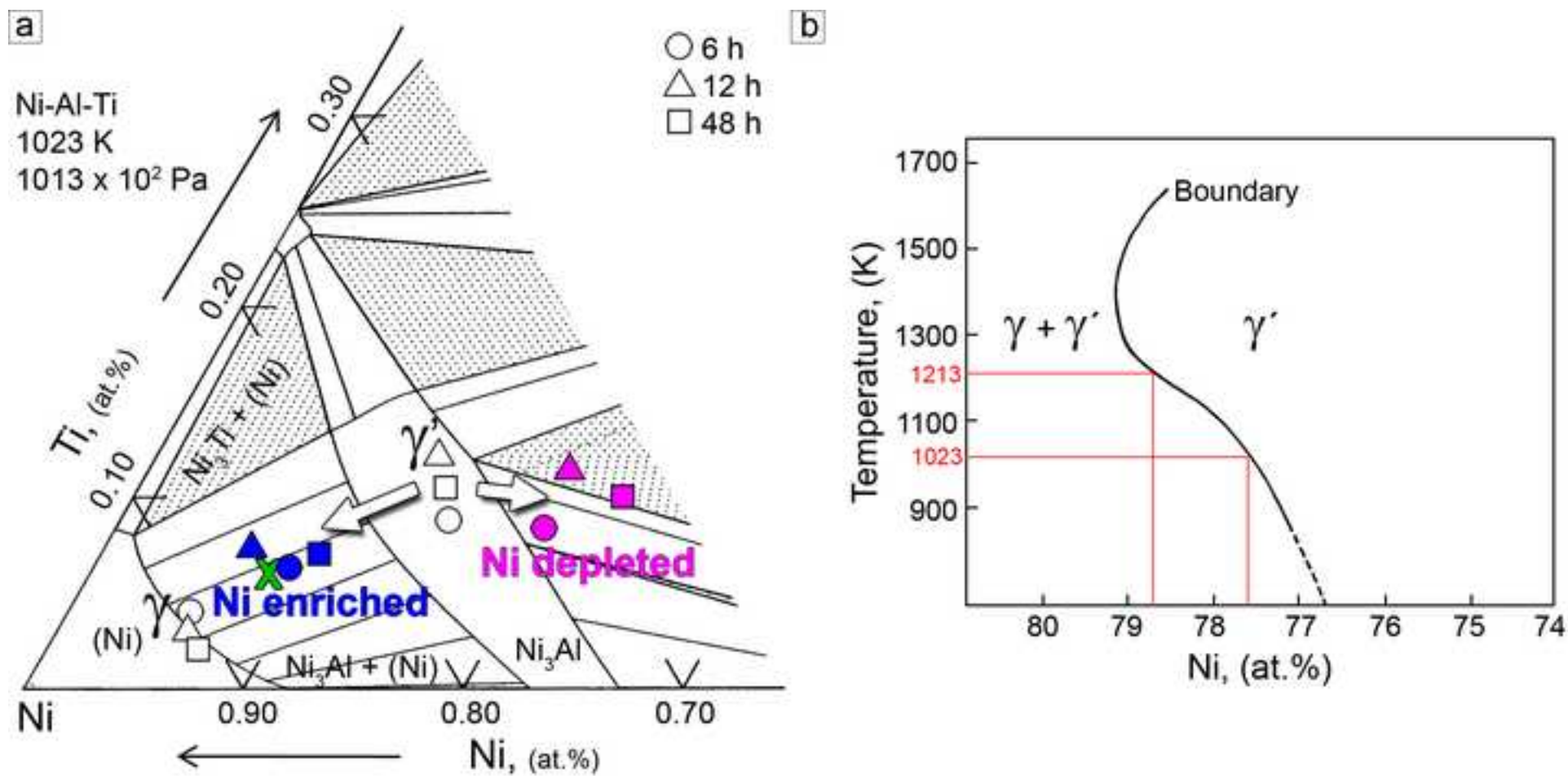


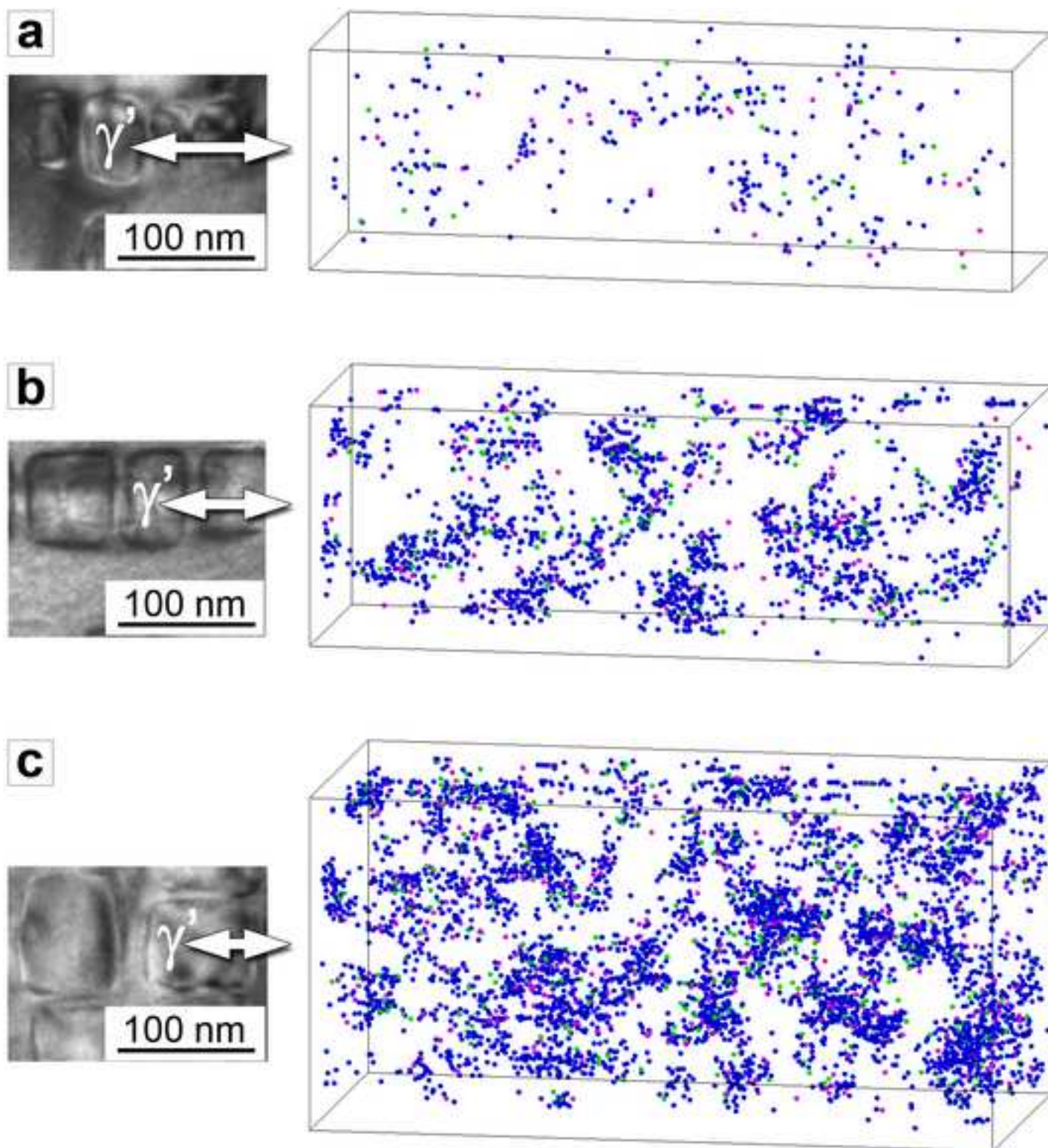






Figure(s)  
[Click here to download high resolution image](#)





> Ni-Al-Ti model alloy to study decomposition of  $\gamma'$  precipitates. > Ni supersaturation of  $\gamma'$  precipitates leads to phase separation phenomenon after heat treatment at 1023 K. > Early stages of decomposition observed as clustering within  $\gamma'$  precipitates.